Editors' Suggestion | Featured in Physics

How Influenza's Spike Motor Works

Falko Ziebert[1,*] and Igor M. Kulić[2,†]
[1]Institute for Theoretical Physics, Heidelberg University, Philosophenweg 19, 69120 Heidelberg, Germany and BioQuant, Heidelberg University, Im Neuenheimer Feld 267, 69120 Heidelberg, Germany
[2]Institut Charles Sadron UPR22-CNRS, 67034 Strasbourg, France and Institute Theory of Polymers, Leibniz-Institute of Polymer Research, D-01069 Dresden, Germany

(Received 5 October 2020; accepted 15 April 2021; published 28 May 2021)

While often believed to be a passive agent that merely exploits its host's metabolism, the influenza virus has recently been shown to actively move across glycan-coated surfaces. This form of enzymatically driven surface motility is currently not well understood and has been loosely linked to burnt-bridge Brownian ratchet mechanisms. Starting from known properties of influenza's spike proteins, we develop a physical model that quantitatively describes the observed motility. It predicts a collectively emerging dynamics of spike proteins and surface-bound ligands that combined with the virus' geometry give rise to a self-organized rolling propulsion. We show that in contrast to a Brownian ratchet, the rotary spike drive is not fluctuation driven but operates optimally as a macroscopic engine in the deterministic regime. The mechanism also applies to relatives of influenza and to man-made analogs like DNA monowheels and should give guidelines for their optimization.

DOI: 10.1103/PhysRevLett.126.218101

One of humanity's greatest inventions is the wheel. While reflecting on why nature overlooked wheeled propulsion, it caught us by surprise that the wheel was rolling in nature eons ago: The common influenza virus uses its whole capsid as a motorized surface rolling machine [1,2]; see Fig. 1(a). The reason for this fundamental discovery of Sakai *et al.* staying almost unnoticed (with few exceptions [3,4]) is possibly rooted in our lack of understanding of its underlying physical mechanism.

Being such an omnipresent molecular adversary, the influenza virus (IV) has been extensively characterized [5–8]. The two spike proteins responsible for IV-A's interaction with the host membrane are hemaglutinin (HA) and neuraminidase (NA); see Fig. 1(b). While in certain influenza subtypes (like IV-C), these two proteins are fused together [9], in general they are distinct ∼10-nm-sized entities performing two mutually competing functions: HA binds sialic acid residues of glycopeptides and lipids coating our cells [Figs. 1(b) and 1(c)]. NA, in turn, acts antagonistically and degrades the contacts with the glycan substrate by hydrolytically cutting the same sialic acid residue that HA binds to; see Fig. 1(d). The residue located at the ends of branched glycans can be either bound by one HA or one NA molecule, but for steric reasons not to both at the same moment. Inhibition of HA abolishes virus binding to glycans [10], while NA inhibition abolishes its motility [2,3].

While most textbooks depict influenza as spheroidal, its aspect ratio is in fact highly polymorphic, and during human infection the majority of the virus mass comes in filamentous form [11,12]. The reason for their filamentous shape with lengths from 1 to 300 μm [11] is debated, since most evolutionary arguments favor the sphere (e.g., volume-to-surface ratio and stability [13] or uptake dynamics [14]). Although previously speculated [15] that elongated viruses could self-propel like man-made actively

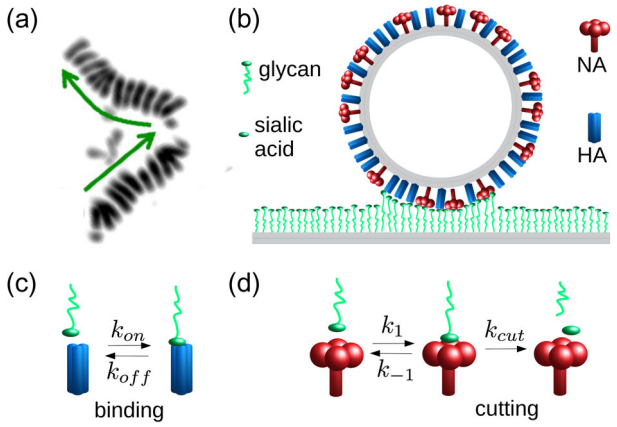

FIG. 1. Rolling influenza, its surface structure, and activity. (a) Superimposed snapshots of a rolling elongated IV-C (taken from Ref. [2]), the green arrows indicating the rolling direction. (b) An IV cross section showing its surface covered with two kinds of spike proteins: hemaglutinin (HA, blue) and neuraminidase (NA, red). The substrate (cell's surface) is covered with glycans exposing a sialic acid residue (green, both not to scale). (c) HA binds to and unbinds from glycan via the sialic acid with rates k_{on}, k_{off}. (d) NA transiently binds with a Michaelis constant $K_M = (k_{-1} + k_{\mathrm{cut}})/k_1$, and hydrolytically cuts the sialic residues with a rate k_{cut}, making the glycans inactive for HA binding.

rolling fibers [16], it was only the work of Sakai *et al.* [2] that found direct evidence and suggests that the elongated form is in fact advantageous for robust directionally persistent motion.

Beyond IV, interestingly DNA nanotechnology has developed synthetic rollers termed DNA monowheels [17–19] that use a similar design principle—namely, linkers and their digestion. So how does influenza, and the motif of "bridging and cutting," generate the force necessary for the rolling motion? Starting from basic known aspects, we develop a model suggesting that it is not a burnt-bridge fluctuation-driven mechanism, but that virus motion is deterministic in nature, macroscopically robust, and in fact, close to inevitable.

The mechanism.—Consider the interface where the viral capsid and the glycan-coated substrate surface meet. In this nanoscopic region, glycan chains at a high concentration G_0 (well in excess to spike proteins; see the estimates below) are constantly binding to and unbinding from the HA proteins and in turn elongating to a length l. Once bound with dissociation constant K_d, they gain a free energy $k_BT\ln(G_0/K_d)$. On the other hand, they pay a stretching energy $E_{\rm el}(\phi) = (S/2)l^2 \approx (R^2S/8)\phi^4$ which, due to the curvature of the capsid, depends on the angle ϕ measured from the virus symmetry axis and its radius R ($\simeq$50 nm for IV); see Fig. 2(a) top panel. Chains bound to NA are short-lived and neglected here for simplicity. We consider the glycan chain as an ideal linear spring with spring constant $S \sim 0.01$–$1 k_BT/\text{nm}^2$ (a typical range for polymers of few nm length) and neglect compression; more details are given in the Supplemental Material [20]. The balance of the two energy terms then sets the angular size $\phi_c = [\ln(G_0/K_d)8k_BT/(SR^2)]^{1/4}$ of the contact zone $\phi \in [-\phi_c, \phi_c]$.

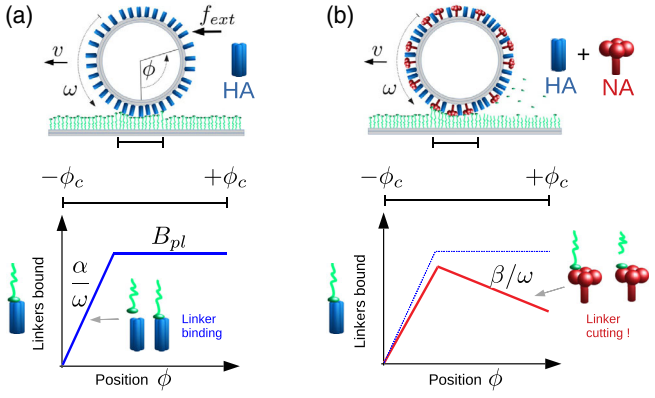

FIG. 2. The double-gradient mechanism of motion maintained by the distribution of bound HA-glycans links. (a) Top: A virus rolling with constant angular frequency ω due to an externally applied force $f_{\rm ext}$. Bottom: The distribution of bound HA-glycans $B(\phi)$ within the contact interval $[-\phi_c, \phi_c]$ has two regions—a sharp increase (with slope α/ω) in the rolling direction followed by a plateau $B = B_{\rm pl}$. (b) Top: self-rolling due to enzymatic activity of NA, cutting away the sialic acid residues. Bottom: In this case, $B(\phi)$ has a negative slope (β/ω) instead of the plateau at the rear.

The stretching force $F_{\rm el} = -(\partial/\partial l)E_{\rm el}$ of a single stretched linker gives rise to a torque $\propto SR^2(1-\cos\phi)\sin\phi \approx \frac{1}{2}SR^2\phi^3$. The linkers have an angular density $\rho_{\rm HA}b(\phi)$ given by the product of the angular density of HA spikes, $\rho_{\rm HA}$, and the angular probability density of each linker being bound, $b(\phi)$. The total torque acting on the capsid is the integral over all bound linkers

$$m = -m_0 \int_{-\phi_c}^{+\phi_c} b(\phi)\phi^3 d\phi = 0. \tag{1}$$

Here, $m_0 = \frac{1}{2}SR^2\rho_{\rm HA}$ is the characteristic torque scale. At typical densities of linkers and angular speeds $\omega \sim 1\ \text{s}^{-1}$ [2], the linker torque dominates all other torques acting on the virus including hydrodynamic dissipation. Therefore, the torque balance $m = 0$ holds.

Denoting the concentration of HA spikes with H_0 and the initial concentration of glycans on the surface as G_0, we have to determine the evolution of the concentration of bound HA-glycan links $B(\phi, t)$ and the glycan concentration $G(\phi, t)$ as functions of the time t and angle $\phi \in [-\phi_c, \phi_c]$. In addition to this binding kinetics, the NA spike enzyme progressively digests the glycan in its vicinity with catalytic velocity $V_{\rm cut}$ and Michaelis constant K_M. Combining these effects and assuming the virus to roll with angular velocity ω, we have

$$\partial_t B + \omega\partial_\phi B = k_{\rm on}G(H_0 - B) - k_{\rm off}B, \tag{2}$$

$$\partial_t G + \omega\partial_\phi G = -k_{\rm on}G(H_0 - B) + k_{\rm off}B - \frac{V_{\rm cut}G}{K_M + G}. \tag{3}$$

Here the terms $\propto \omega$ on the lhs represent the advection of concentrations in the virus fixed frame due to its rotation. The first terms on the rhs are the on and off kinetics of glycan binding, with the kinetic constants satisfying $k_{\rm off}/k_{\rm on} = K_d$. Although the off rate is stretching force [21], and hence, angle dependent, we neglect this effect here for simplicity (see Supplemental Material [20] for the more general case).

Finally, the last term in Eq. (3) represents the Michaelis-Menten-like degradation of free glycans by NA, with a velocity $V_{\rm cut} = k_{\rm cut}N$ set by the cutting rate $k_{\rm cut}$ and enzyme concentration N. Note that this term distinguishes virus spike dynamics from classical collective molecular motors [22,23], where the on-off kinetics is already breaking the detailed balance. Equations (2) and (3), together with $b(\phi) = B/H_0$ satisfying the torque balance, Eq. (1), completely determine the dynamics, and the question is now whether the enzymatic activity can sustain solutions with nonzero ω.

Passive frictional torque.—In a first step, it is instructive to consider the passive case, i.e., in the absence of catalytic

activity ($V_{\rm cut}=0$), where a virus is forced by an external torque to roll with a steady-state angular velocity ω [24]. Related situations have been investigated for cells rolling in external shear flow [25,26] and contraction or sliding motion induced by stochastic linkers [27,28]. At steady state, Eqs. (2) and (3) imply the conservation law $(B+G)'=0$ or $G=G_0-B$ (for homogeneous G_0), allowing us to reduce the problem to

$$\omega B' = k_{\rm on}(G_0-B)(H_0-B)-k_{\rm off}B. \tag{4}$$

For the initial condition $B(-\phi_c)=0$ (rolling to the left), the exact solution is

$$B(\phi)=\frac{C_0-C_1}{2}-\frac{C_1}{\frac{C_0+C_1}{C_0-C_1}e^{\frac{C_1 k_{\rm on}}{\omega}(\phi+\phi_c)}-1}, \tag{5}$$

with constants $C_0=H_0+G_0+K_d$, $C_1=\sqrt{C_0^2-4H_0G_0}$. This profile [cf. the sketch in the bottom panel of Fig. 2(a)] implies an increase of the bound HA-glycan links leveling to a plateau $B_{\rm pl}=(C_0-C_1)/2$ [29]. For simplicity, we approximate the exact profile by two lines: First, in the region of its rapid increase, B is approximated by the slope at the front. For $\phi\in[-\phi_c,\phi_{\rm pl}]$, $B(\phi)=(\alpha/\omega)(\phi+\phi_c)$ with $\phi_{\rm pl}$ the angle where the plateau is reached and the linker binding velocity $\alpha=k_{\rm on}H_0G_0$. The faster the rolling, the shallower the spatial gradient becomes, since the build up of HA-glycan links needs time. Second, for $\phi\in[\phi_{\rm pl},\phi_c]$ we approximate B by its plateau value $B_{\rm pl}$.

With this slope-plateau approximation, Eq. (1) evaluates to

$$m_{\rm diss}(\omega)=-\xi_{\rm diss}\omega, \qquad \xi_{\rm diss}=\frac{m_0}{H_0}\frac{B_{\rm pl}^2}{\alpha}\frac{\phi_c^3}{2}. \tag{6}$$

Hence, this is a frictional torque acting against the motion and linear in ω. The friction constant $\xi_{\rm diss}$ is determined by both the slope and the plateau of the distribution of B as well as the size of the contact interval, which themselves contain all system parameters.

Enzyme activity induces active torque.—The effect of NA activity can be captured perturbatively and leads to an additional contribution to the torque. If enzyme activity is slow compared to the binding kinetics, $\epsilon=V_{\rm cut}/\alpha$ is a small parameter. Expanding $B=B^{(0)}+\epsilon B^{(1)}$ and $G=G^{(0)}+\epsilon G^{(1)}$ in powers of ϵ yields the leading order correction $B^{(1)}=-\alpha f[(\phi+\phi_c)/\omega]$ with

$$f=\frac{H_0-B_{\rm pl}}{K_d+G_{\rm pl}}\frac{G_{\rm pl}}{K_M+G_{\rm pl}} \tag{7}$$

a dimensionless ratio of all concentrations and kinetic constants and $G_{\rm pl}=G_0-B_{\rm pl}$ the plateau of the glycan distribution (in the passive case). The enzymatic activity hence leads to a negative slope $\beta=V_{\rm cut}f$ instead of the plateau [cf. Fig. 2(b)], and insertion into Eq. (1) yields the active torque in the "two-slope" approximation:

$$m_{\rm act}=\frac{p_{\rm act}}{\omega}, \qquad p_{\rm act}=\frac{m_0}{H_0}f\frac{2\phi_c^5}{5}V_{\rm cut}, \tag{8}$$

where $p_{\rm act}$ is the power injected by NA operation. The active torque is positive, it is proportional to $V_{\rm cut}$, and has a $1/\omega$ dependence, unlike the passive one. Note that the two-slope approximation is valid only for $\omega>2k_{\rm on}G_0\phi_c\beta/(\alpha+\beta)$; for very slow rotation, the glycans can be completely cut at the back and a third region has to be considered, as explained in the Supplemental Material [20].

Taken together, the passive and active torques yield the torque balance

$$m_{\rm diss}+m_{\rm act}=0=-\xi_{\rm diss}\omega+p_{\rm act}/\omega \tag{9}$$

implying a pitchfork bifurcation for the steady-state rolling velocity

$$\omega=\pm\sqrt{\frac{p_{\rm act}}{\xi_{\rm diss}}}\propto\phi_c\sqrt{f}\frac{\sqrt{\alpha V_{\rm cut}}}{B_{\rm pl}}. \tag{10}$$

We can compare Eq. (10) to the experiments [2] by inserting typical parameters for IVs: $R=50$ nm and $S\simeq 0.1k_BT/{\rm nm}^2$ imply $\phi_c\simeq 0.5$. Typical concentrations are $G_0=10$ mM, $H_0=1$–$5(\text{we use }2)$ mM [30]. The HA on-off kinetics was characterized [31] yielding $K_d=1$–$5(2)$ mM, $k_{\rm off}=10^{-1}$–$1(1)$ s^{-1}, $k_{\rm on}=0.01$–$1(0.5)$ mM^{-1} s^{-1}, and NA's enzymatic activity [32] to yield $K_M=14.3$ mM, $k_{\rm cat}\simeq 15\,{\rm s}^{-1}$, implying $V_{\rm cut}=15\,{\rm mM\,s}^{-1}$ for a typical NA concentration of $N=1$ mM. Using these values, we get $\omega\simeq 0.4$ s^{-1}, which compares well to Ref. [2] where virus speeds of $v=10$–30 nm/s were reported, corresponding to $\omega=v/R\simeq 0.2$–0.6 s^{-1}.

Stochasticity.—To scrutinize the robustness of the mechanism, we implemented stochastic reaction kinetics using the Gillespie algorithm [33]. For the latter, the virus cross section was assumed to present a number of $n_{\rm vir}$ discrete binding sites per contact interval. Larger $n_{\rm vir}$ correspond to more elongated viruses with more linkers per angle, with $n_{\rm vir}\to\infty$ the deterministic limit. The virus position is updated in each step in accordance to the vanishing torque condition.

Figure 3(a) compares the two-slope theory to a numerical solution of the continuum model and stochastic simulations. While in the stochastic implementation the virus inverts its rolling direction occasionally, it is evident from the figure that the mechanism is robust against a finite number of binding site effects. It nevertheless works best (rolling is fastest) for the "macroscopic" (continuum) case, in contrast to the classical burnt-bridge mechanism. Figure 3(b) shows a stochastic simulation highlighting the

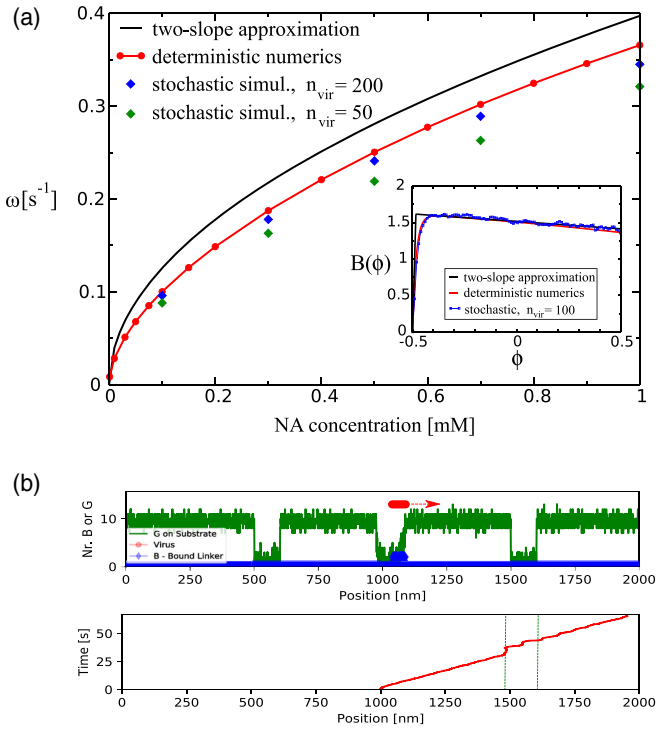

FIG. 3. (a) Rolling velocity and bound linker profile in the continuum vs the stochastic model. Shown is the rolling frequency ω as a function of the enzymatic activity (NA concentration): approximate theory (black), numerical solution of the continuum model (red), and stochastic implementation (symbols). Inset: $B(\phi)$ profiles in the three cases for $N = 0.1$ mM (stochastic profile averaged over 50.000 Gillespie moves). (b) Example stochastic simulation. The upper panel shows a snapshot of the bound linker (blue) and the glycan (green) distributions and the lower panel the trajectory. The surface-bound glycans were locally depleted (marked in the trajectory by the green vertical lines), but the rolling motion persists.

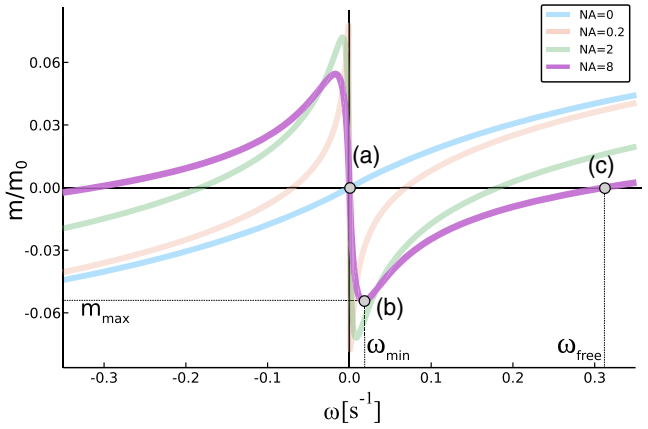

FIG. 4. Torque-angular velocity relation displaying several characteristic points. (a) Static state: no motion and no torque. (b) The system operates at the stalling torque $m_{\max}$ at a minimal critical speed $\omega_{\min}$. (c) The virus runs torque-free at its intrinsic speed ω_{free}.

mechanism's robustness against perturbations in the glycan distribution for the case of a surface displaying small, almost glycan-depleted regions. Although the virus is slowed down in the depleted zones, its motion persists.

Torque-angular velocity relation.—Adding an opposing external torque to the torque balance Eq. (9), we obtain the approximate force-velocity ("motor") relation

$$m(\omega) \approx \xi_{\text{diss}}\omega - \frac{p_{\text{act}}}{\omega} \tag{11}$$

valid for sufficiently large ω. Figure 4 shows corresponding numerically obtained curves for different NA activity for the full frequency range. Equation (11) corresponds to the curve from point B toward C and beyond. For an approximate analytical form for the full curve and its deeper analysis, we refer to the Supplemental Material [20] and Ref. [34].

A synthetic relative: The DNA monowheel.—The generic mechanism employed by IV is the interplay of binding and digestion of linkers, the enzymatic activity transforming the plateau of the linker distribution into a negative slope. One can imagine other reaction pathways to result in a similar "polarization." In fact, a synthetic variant of the generic mechanism was recently implemented using DNA nanotechnology [17,18]. There, the surface of silica particles was covered with DNA sequences that form heteroduplexes with complementary ribonucleic acid (RNA) strands coated on a surface. The motion of the particles (termed *monowheels* in Ref. [17]) was initiated by adding Ribonuclease-H, which selectively hydrolyzes hybridized RNA (the bound linkers, B in our notation) but not single-stranded RNAs (i.e., free linkers, G).

This variant can be easily cast into our theoretical framework: As the enzyme RNase-H does not destroy the free linkers but instead the *bound* ones, the enzymatic term is absent in Eq. (3), but its analog $-V_{\text{cut}}B/(K_M + B)$ has to be added to Eq. (2). Analyzing along the same lines yields an active torque as in Eq. (8) but with $f = B_{\text{pl}}/(K_M + B_{\text{pl}})$. Again inserting numbers ([17,18,35–37]; see Supplemental Material [20] for details), one gets $B_{\text{pl}} \gg K_M$, hence, $f \simeq 1$ and, as the passive torque has the same dependence as before,

$$\omega = \pm\frac{2}{\sqrt{5}}\frac{\sqrt{\alpha V_{\text{cut}}}}{B_{\text{pl}}}\phi_c, \tag{12}$$

and finally, $\omega \simeq 10^{-2}$ s^{-1}. This again fits well to the experimentally observed velocity of 30 nm/s [17] implying $\omega \simeq 10^{-2}$ s^{-1}.

Discussion.—The double-gradient mechanism described here is very robust and can give rise to large propulsion speeds even for weak enzymatic activity. Importantly, it is not a simple bridge burning as recently hypothesized for both IV and the DNA wheel [2,18]. Although bridge

burning can be operative for certain IV-A strains that show phase separation of NA and HA spikes [38], these lack rolling and move much slower than reported in Refs. [1,2]. In burnt-bridge models [39,40], the random walker destroys the "bridges" it walks on, and only the prohibited backstepping leads to directed motion on self-avoiding paths. Such models, like most other Brownian motors [23,41], are inherently fluctuation driven, and increasing the density of linkers implies a slowdown of motion. In contrast, the mechanism discussed here relies on the self-organized "internal" polarization of the linker distribution within the contact zone and works optimally in the macroscopic regime, similar to collective molecular motors [22,23]. The mechanism is robust [cf. Fig. 3(b)] but not self-avoiding and unidirectional, since the roller can run in reverse direction even if its trail is substantially depleted behind. It responds to existing surface gradients, but much less than a burnt-bridge walker, giving the virus—controlling its contact zone—a higher motile autonomy in the evolutionary race with its host, controlling the rest of the substrate. How the "delicate balance" [4] of NA vs HA and its adaptation orchestrates the mechanism in detail should be explored more in the future.

With influenza, we are facing an underestimated, smart adversary that in contrast to classical virology dogmas displays a "metabolism" on its surface, providing it with a motile organelle that emerges from geometry and the self-organization of its spike proteins. The mechanism should apply to relatives of influenza bearing enzymatic spike proteins, including torovirus and some betacoronaviruses [42].

We thank Jens-Uwe Sommer, Ulrich Schwarz, Felix Frey, and Pedro Soria for discussions. I. M. K. thanks the Leibniz-Institute IPF Dresden for hospitality.

*ziebert@thphys.uni-heidelberg.de
†kulic@unistra.fr

[1] T. Sakai, S. I. Nishimura, T. Naito, and M. Saito, Sci. Rep. **7**, 45043 (2017).
[2] T. Sakai, H. Takagi, Y. Muraki, and M. Saito, J. Virol. **92**, e01522 (2018).
[3] H. Guo *et al.*, PLoS Pathogens **14**, e1007233 (2018).
[4] E. de Vries, W. Du, H. Guo, and C. A. M. de Haan, Trends Microbiol. **28**, 57 (2020).
[5] J. N. Varghese, W. G. Laver, and P. M. Colman, Nature (London) **303**, 35 (1983).
[6] D. C. Wiley and J. J. Skehel, Annu. Rev. Biochem. **56**, 365 (1987).
[7] S. J. Gamblin and J. J. Skehel, J. Biol. Chem. **285**, 28403 (2010).
[8] D. Dou, R. Revol, H. Östbye, H. Wang, and R. Daniels, Front. Immunol. **9**, 1581 (2018).
[9] M. Wang and M. Veit, Protein Cell **7**, 28 (2016).
[10] E. Spackman and I. Sitaras, in *Animal Influenza Virus*, edited by E. Spackman (Humana, New York, 2020), Vol. 2123.
[11] M. D. Badham and J. S. Rossman, Curr. Clin. Microbiol. Rep. **3**, 155 (2016).
[12] B. Dadonaite, S. Vijayakrishnan, E. Fodor, D. Bhella, and E. C. Hutchinson, J. Gen. Virol. **97**, 1755 (2016).
[13] R. Zandi, D. Reguera, R. F. Bruinsma, W. M. Gelbart, and J. Rudnick, Proc. Natl. Acad. Sci. U.S.A. **101**, 15556 (2004).
[14] F. Frey, F. Ziebert, and U. S. Schwarz, Phys. Rev. Lett. **122**, 088102 (2019).
[15] A. Bazir, A. Baumann, F. Ziebert, and I. M. Kulić, Soft Matter **16**, 5210 (2020).
[16] A. Baumann, A. Sánchez-Ferrer, L. Jacomine, P. Martinoty, V. Le Houerou, F. Ziebert, and I. M. Kulić, Nat. Mater. **17**, 523 (2018).
[17] K. Yehl, A. Mugler, S. Vivek, Y. Liu, Y. Zhang, M. Fan, E. R. Weeks, and K. Salaita, Nat. Nanotechnol. **11**, 184 (2016).
[18] A. T. Blanchard, A. S. Bazrafshan, J. Yi, J. T. Eisman, K. M. Yehl, T. Bian, A. Mugler, and K. Salaita, Nano Lett. **19**, 6977 (2019).
[19] A. Bazrafshan, T. A. Meyer, H. Su, J. M. Brockman, A. T. Blanchard, S. Piranej, Y. Duan, Y. Ke, and K. Salaita, Angew. Chem., Int. Ed. Engl. **59**, 9514 (2020).
[20] See Supplemental Material at http://link.aps.org/supplemental/10.1103/PhysRevLett.126.218101 for more information on the used approximations and the full force-angular velocity relation.
[21] E. Evans and K. Ritchie, Biophys. J. **72**, 1541 (1997).
[22] F. Jülicher and J. Prost, Phys. Rev. Lett. **75**, 2618 (1995).
[23] F. Jülicher, A. Ajdari, and J. Prost, Rev. Mod. Phys. **69**, 1269 (1997).
[24] Note that we apply a quasistatic approximation here, neglecting that the contact zone can become asymmetric at larger frequencies [25], leading to additional dissipation at the rear end where chains do not have sufficient time to detach.
[25] E. F. Krasik and D. A. Hammer, Biophys. J. **87**, 2919 (2004).
[26] C. B. Korn and U. S. Schwarz, Phys. Rev. E **77**, 041904 (2008).
[27] S. Walcott and S. X. Sun, Phys. Rev. E **82**, 050901(R) (2010).
[28] P. Sens, Europhys. Lett. **104**, 38003 (2013).
[29] Note that the bound linker profile in the static case $\omega = 0$ is a rectangular function with B_{pl} in the contact interval due to the neglection of angle dependence of the off rate.
[30] The volume concentrations G_0, H_0, and N (in $M = \mathrm{mol/l}$) can be estimated from typical volumes per molecule $V = A\delta$, with $A \sim 100$–$500\ \mathrm{nm}^2$ (for glycans and spike proteins, respectively) the area per molecule and $\delta \sim 1$ nm its typical height fluctuation from the surface.
[31] N. K. Sauter *et al.*, Biochem. **28**, 8388 (1989); **31**, 9609 (1992).
[32] S. E. Adams, N. Lee, V. Y. Lugovtsev, A. Kan, R. P. Donnelly, and N. A. Ilyushina, Antiviral research **169**, 104539 (2019).
[33] D. T. Gillespie, J. Phys. Chem. **81**, 2340 (1977).
[34] P. Soria, F. Ziebert, and I. M. Kulić (to be published).

[35] K. Bielec, K. Sozanski, M. Seynen, Z. Dziekan, P. Rein ten Wolde, and R. Holyst, Phys. Chem. Chem. Phys. **21**, 10798 (2019).
[36] T. Strunz, K. Oroszlan, R. Schäfer, and H.-J. Güntherodt, Proc. Natl. Acad. Sci. U.S.A. **96**, 11277 (1999).
[37] S. Fang, H. J. Lee, A. W. Wark, H. M. Kim, and R. M. Corn, Anal. Chem. **77**, 6528 (2005).
[38] M. D. Vahey and D. A. Fletcher, eLife **8**, e43764 (2019).
[39] J. Mai, I. M. Sokolov, and A. Blumen, Phys. Rev. E **64**, 011102 (2001).
[40] T. Antal and P. L. Krapivsky, Phys. Rev. E **72**, 046104 (2005).
[41] P. Reimann, Phys. Rep. **361**, 57 (2002).
[42] R. J. de Groot, Glycoconjugate Journal **23**, 59 (2006).